RSC Advances

This article can be cited before page numbers have been issued, to do this please use: X. Lin, J. Hou, S. Jiang, Z. Lin, M. Wang and G. Che, *RSC Adv.*, 2015, DOI: 10.1039/C5RA22110B.

View Article Online
DOI: 10.1039/C5RA22110B

RSC Advances

ARTICLE

Received 00th January 20xx,
Accepted 00th January 20xx
DOI: 10.1039/x0xx00000x
www.rsc.org/

A Z-Scheme Visible-Light-Driven $Ag/Ag_3PO_4/Bi_2MoO_6$ photocatalyst: Synthesis and Enhanced Photocatalytic Activity

Xue Lin, Jing Hou, Shanshan Jiang, Zhe Lin, Miao Wang, and Guangbo Che *

A $Ag/Ag_3PO_4/Bi_2MoO_6$ hybrid was successfully prepared for the first time via an in-situ precipitation method. The as-prepared $Ag/Ag_3PO_4/Bi_2MoO_6$ hybrid included Ag_3PO_4 nanoparticles (NPs) as well as Ag NPs assembling on the surface of Bi_2MoO_6 nanosheets. Under visible light irradiation (λ > 420 nm), the $Ag/Ag_3PO_4/Bi_2MoO_6$ hybrid photocatalyst degraded rhodamine B (Rh B) efficiently and showed much higher photocatalytic activity than pure Ag_3PO_4, Bi_2MoO_6, Ag/Ag_3PO_4, Ag/Bi_2MoO_6, or Ag_3PO_4/Bi_2MoO_6. It was elucidated that the excellent photocatalytic performance of $Ag/Ag_3PO_4/Bi_2MoO_6$ for the degradation of Rh B under visible light could be ascribed to the efficient separation of photogenerated electrons and holes through the Z-scheme system composed of Ag_3PO_4, Ag and Bi_2MoO_6, in which the Ag NPs acted as the charge transmission-bridge. The quenching effects of different scavengers illustrated that $O_2^{\bullet-}$ and h^+ played the major role in the Rh B degradation.

1. Introduction

Semiconductors-based photocatalysis is a promising environmental friendly technology to solve the environmental contamination issues [1-4]. Exploring high-efficiency semiconductor photocatalysts is of great importance to transform this technology into practical applications. Unfortunately, most widely applied semiconductor photocatalysts, such as TiO_2, ZnO, SiO_2, and CuO [5-9] are just active under UV-light irradiation, which greatly hinders their further applications under solar light. Therefore, great efforts have been made to synthesize efficient visible-light-driven photocatalysts such as $BiVO_4$, Bi_2WO_6, Bi_2MoO_6, and BiOX (X = Cl, Br, or I) [10-15]. Among these visible-light catalysts, Bi_2MoO_6 has been found to reveal excellent visible-light-driven photocatalytic activity for water splitting and/or for the degradation of organic contaminants [16,17]. However, further research on the improvement of the photocatalytic efficiency of Bi_2MoO_6 is still indispensable due to its poor quantum yield. Among a variety of methods, the constructions of hybrid photocatalysts and heterostructures have been shown to be effective approaches for enhancing photocatalytic performance for the degradation of organic contaminants. So far, a variety of Bi_2MoO_6-based photocatalysts such as TiO_2/Bi_2MoO_6 [18], C/Bi_2MoO_6 [19], graphene/Bi_2MoO_6 [20], $Bi_{3.64}Mo_{0.36}O_{6.55}/Bi_2MoO_6$ [21], $ZnTiO_3/Bi_2MoO_6$ [22], $Ag/AgBr/Bi_2MoO_6$ [23], and g-C_3N_4/Bi_2MoO_6 [24] have been fabricated for improving the photocatalytic property of Bi_2MoO_6.

Ag_3PO_4 is well known as a photosensitive material and regarded as an appropriate candidate for the construction of hybrid photocatalysts with other semiconductors [25,26]. Zhang and co-workers reported the Ag_3PO_4/Bi_2MoO_6 photocatalyst, which was fabricated by covering the surface of spherical Bi_2MoO_6 with Ag_3PO_4 nanoparticles through deposition–precipitation process [27]. This hybrid showed remarkably high photocatalytic efficiency for the degradation of rhodamine B (Rh B) and methyl blue (MB) under visible light irradiation. However, Ag_3PO_4 is subject to stability issues because it is prone to photoreduction and decomposition if no sacrificial reagent is supplied, which greatly hinders its practical application in the environmental management. It has been reported that elemental silver Ag^0 on the surface of Ag_3PO_4 may act as an electron acceptor to enhance the charge separation and prevent the reductive decomposition of Ag_3PO_4 [28]. In addition, metallic silver species can significantly improve the visible light absorption efficiency due to the effect of surface plasmon resonance. In addition, with more and more attention has been paid to the mechanism of Ag/Ag_3PO_4-based photocatalysts, the by-product Ag has been found to be a charge transmission bridge in the Ag/Ag_3PO_4-based Z-scheme systems. It has been reported that these Z-scheme systems can not only facilitate the charge separation but also retain the high reducibility and oxidability of the remaining electrons and holes for the corresponding photocatalysts [28-30]. Recently, there are a few reports on the photocatalytic activity evaluation of Ag/Ag_3PO_4-based Z-scheme systems, for instance $Ag/Ag_3PO_4/SiC$ [28], $Ag/Ag_3PO_4/g\text{-}C_3N_4$ [29], and $Ag/Ag_3PO_4/WO_{3-x}$ [30]. Thus, by combining Bi_2MoO_6 and Ag/Ag_3PO_4 particles to constitute a Z-scheme photocatalyst, both the utilization of visible light and the surface–interface charge transfer efficiency of photo-generated carriers could be enhanced. However, until now, there is few report focusing on the assembly of Bi_2MoO_6 nanosheet with Ag/Ag_3PO_4 NPs. Furthermore, no attention has been paid to the mechanism of $Ag/Ag_3PO_4/Bi_2MoO_6$ photodegradation process under visible light irradiation, which has remained unclear to date.

Herein, we report a successful attempt at the fabrication of $Ag/Ag_3PO_4/Bi_2MoO_6$ hierarchical nanostructures via an in-situ facile in-situ precipitation method, and the photocatalytic activity of these nanostructures was investigated by measuring the degradation of rhodamine B (Rh B) under visible light (λ > 420 nm). Furthermore, the photocatalytic mechanism of the $Ag/Ag_3PO_4/Bi_2MoO_6$ hybrid was investigated via reactive species trapping experiments. Finally, the stability of the $Ag/Ag_3PO_4/Bi_2MoO_6$ hybrid photocatalyst was also examined.

Key Laboratory of Preparation and Application Environmentally Friendly Materials of Ministry of Education, Jilin Normal University, Siping 136000, P. R. China
E-mail:jlsdlinxue@126.com; Fax: +86 434 329 1890; Tel: +86 156 9434 9717
See DOI: 10.1039/x0xx00000x

View Article Online
DOI: 10.1039/C5RA22110B

2. Experimental

2.1 Preparation of photocatalysts

2.1.1 Preparation of Bi_2MoO_6 nanosheets

All reagents for synthesis and analysis were commercially available and used without further treatments. The Bi_2MoO_6 nanosheets were synthesized through a facile hydrothermal method. Briefly, a solution of $Bi(NO_3)_3$ (0.40 mol/L, 5 mL H_2O) was stirred for 30 min. Then, $(NH_4)_6Mo_7O_{24}$ (0.20 mol/L, 5 mL H_2O) was added to the suspension, which was stirred magnetically for another 30 min. After carefully adjusting the pH value of 3 using 25 wt% $NH_3{\cdot}H_2O$ solution, the mixed solution was transferred into a 20 mL Teflon-lined steel autoclave, which was heated in an oven at 160 °C for 24 h. Then the system was allowed to cool to room temperature naturally. At last, the obtained samples were collected and washed with ethanol and distilled water several times, and dried at 70 °C for 2 h.

2.1.2 Preparation of $Ag/Ag_3PO_4/Bi_2MoO_6$ photocatalyst

The $Ag/Ag_3PO_4/Bi_2MoO_6$ hybrid photocatalyst was synthesized through an in-situ precipitation method at room temperature. In a typical process, Bi_2MoO_6 nanosheets (500 mg) were dispersed in 100 mL deionized water by ultrasound for 30 min, and then 50 mL 0.0075 M $AgNO_3$ aqueous solution was dropped into the Bi_2MoO_6 dispersed solution. After stirring for 15 min, a 50 mL of 0.0025 M Na_3PO_4 aqueous solution was added to the above solution drop by drop under magnetic stirring. The pH value was adjusted to 3 by adding 1.0 M NaOH. The resulting suspension was stirred in the dark for another 30 min. Then, the suspension was irradiated by a 300 W Xe lamp equipped with an optical cut-off filter (λ > 420 nm) for 30 min. Finally, the precipitate was washed with deionized water for 3 times and collected by centrifugation, and then dried at 60 °C in the vacuum drying oven. The theoretical value of Ag_3PO_4 loading amount was 10 wt%. For comparison, pure Ag_3PO_4, Ag/Bi_2MoO_6, Ag/Ag_3PO_4, and Ag_3PO_4/Bi_2MoO_6 samples were prepared under the same conditions.

2.2. Characterization of photocatalysts

The crystal structures of the samples were characterized by X-ray diffraction (XRD) on a Rigaku (Japan) D/max 2500 X-ray diffractometer (Cu K_α radiation, λ = 0.154 18 nm). The morphologies and structure details of the as-synthesized samples were detected using field emission scanning microscopy (SEM, JSM-6510) and transmission electron microscopy (TEM, JEM-2100F). X-ray photoelectron spectroscopy (XPS) analysis was performed with an ESCALa-b220i-XL electron spectrometer (VGScientific, England) using 300 W Al K_α radiation. The optical properties were obtained by the photoluminescence (PL) measurement using HR800 LabRam Infinity Spectro photometer excited by a continuous He-Cd laser with a wavelength of 325 nm at a power of 50 mW. The UV-vis diffuse reflectance spectra (DRS) were recorded using a scan UV-vis spectrophotometer (UV-2550).

2.3. Photocatalytic activities studies

The photocatalytic properties of the as-prepared samples were evaluated using Rh B as a model compound. The Rh B is a very stable compound, which has been used widely as a representative reaction for examining the performance of numerous visible light active photocatalysts. In experiments, the Rh B solution (0.01 mmol·L^{-1}, 100 mL) containing 0.02 g of photocatalyst were mixed in a pyrex reaction glass. A 300 W Xe lamp (λ > 420 nm) was employed to provide visible light irradiation. A 420 nm cut-off filter was inserted between the lamp and the sample to filter out UV light (λ < 420 nm). Prior to visible light illumination, the suspension was strongly stirred in the dark for 40 min. Then the solution was exposed to visible light irradiation under magnetic stirring. At given time intervals, 4 mL of the suspension was periodically collected and analyzed after centrifugation. The Rh B concentration was analyzed by a UV-2550 spectrometer to record intensity of the maximum band at 552 nm in the UV-vis absorption spectra.

2.4 Active species trapping experiments

For detecting the active species during photocatalytic reactivity, some sacrificial agents, such as 2-propanol (IPA), disodium ethylenediamine tetraacetic acid (EDTA-2Na), and 1,4-benzoquinone (BQ) were used as the hydroxyl radical (•OH) scavenger, hole (h^+) scavenger and superoxide radical ($O_2^{\bullet-}$) scavenger, respectively. The method was similar to the former photocatalytic activity test with the addition of 1 mmol of quencher in the presence of Rh B.

3. Results and discussion

Fig. 1 displays the XRD pattern of the $Ag/Ag_3PO_4/Bi_2MoO_6$ hybrid photocatalyst, together with those of pure Ag_3PO_4, Bi_2MoO_6, Ag/Bi_2MoO_6, Ag/Ag_3PO_4, and Ag_3PO_4/Bi_2MoO_6 samples. As can be seen in Fig. 1, Ag_3PO_4 is a cubic phase (JCPDS NO. 06-0505), while Bi_2MoO_6 is an orthorhombic crystal (JCPDS NO. 21-0102). It is observed that no peaks assigned to Ag^o were found in the as-prepared $Ag/Ag_3PO_4/Bi_2MoO_6$, Ag/Ag_3PO_4, and Ag/Bi_2MoO_6 samples, owing to its low amount. Moreover, the changes of all diffractions and lattice parameters were not detectable, which indicates that Ag related species resided in the lattice sites and have no separate phase. No obvious peaks of the Ag_3PO_4 phases were detected in the patterns of $Ag/Ag_3PO_4/Bi_2MoO_6$ and Ag_3PO_4/Bi_2MoO_6, suggesting that all the as-synthesized composites possess the same crystal structure. This may be resulted from the low concentration or small crystal size of Ag_3PO_4.

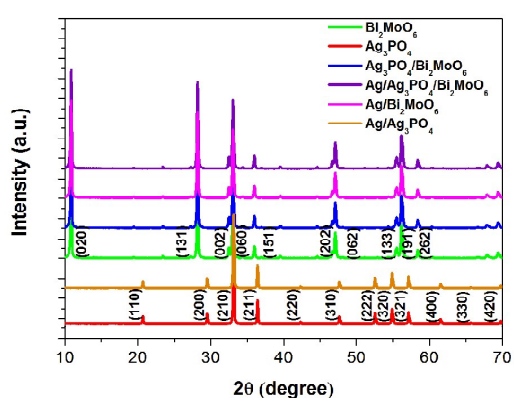

Fig. 1 XRD patterns of Ag_3PO_4, Bi_2MoO_6, Ag/Bi_2MoO_6, Ag/Ag_3PO_4, Ag_3PO_4/Bi_2MoO_6, and $Ag/Ag_3PO_4/Bi_2MoO_6$ hybrids.

In order to confirm the existence of metallic Ag and Ag_3PO_4, XPS technology has been employed to analyze the surface element composition and chemical state of $Ag/Ag_3PO_4/Bi_2MoO_6$, and the obtained results are shown in Fig. 2. From Fig. 2a, the Ag 3d peaks of $Ag/Ag_3PO_4/Bi_2MoO_6$ have separated as Ag^+ peaks and Ag^0 peaks. The peaks at 367.1 and 373.1 eV are attributed to Ag^0 of Ag_3PO_4 [28], indicating existence of metallic Ag on the surface of $Ag/Ag_3PO_4/Bi_2MoO_6$ sample. The peaks at 366.4 and 372.3 eV are assigned to Ag^+ of Ag_3PO_4 [28]. A broad peak in the range of 129 to 134 eV of the P 2p spectrum (Fig. 2b) is observed for the $Ag/Ag_3PO_4/Bi_2MoO_6$ sample which is corresponding to the

View Article Online
DOI: 10.1039/C5RA22110B

phosphorus of Ag_3PO_4 [29]. The results give solid evidence of the formation of metallic Ag and Ag_3PO_4. The Bi 4f fine XPS spectrum of the sample is shown in Fig. 2c. XPS signals of Bi 4f are observed at binding energies at about 162.9 eV (Bi $4f_{7/2}$) and 157.5 eV (Bi $4f_{5/2}$), ascribed to Bi^{3+} [27]. The characteristic spin-orbital splitting photoelectrons for Mo 3d (234.8 and 231.6 eV) indicate a six-valent oxidation state for Mo^{6+} [27] (Fig. 2d).

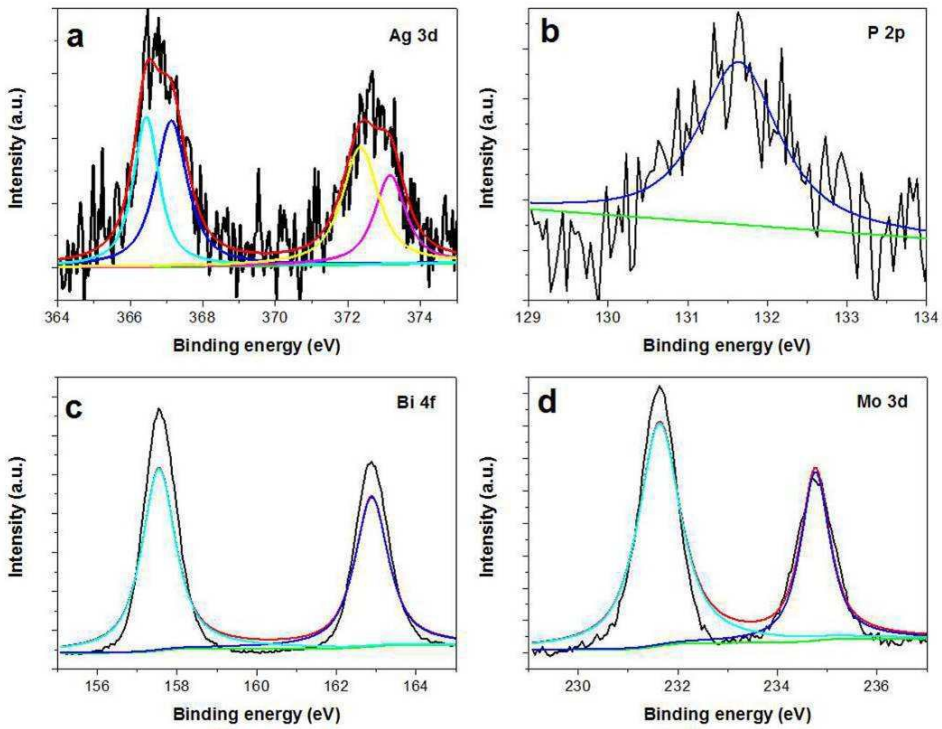

Fig. 2 XPS spectra of the as-obtained $Ag/Ag_3PO_4/Bi_2MoO_6$ sample: (a) Ag 3d spectrum, (b) P 2p spectrum, (c) Bi 4f, (d) Mo 3d spectrum.

The SEM images of Bi_2MoO_6, Ag/Bi_2MoO_6, Ag_3PO_4/Bi_2MoO_6 and $Ag/Ag_3PO_4/Bi_2MoO_6$ samples are revealed in the Fig. S1. The as-prepared Bi_2MoO_6 particles are composed of nanosheets with average sizes of about 100 nm and thickness of tens of nanometers (Fig. S1a). The Ag/Bi_2MoO_6, Ag_3PO_4/Bi_2MoO_6, and $Ag/Ag_3PO_4/Bi_2MoO_6$ samples display a similar morphology to pure Bi_2MoO_6 (Fig. S1b-d), indicating that low amount Ag_3PO_4 and Ag loading did not have any influence on the morphology of Bi_2MoO_6 crystals. Moreover, the component and connection of $Ag/Ag_3PO_4/Bi_2MoO_6$ were investigated by TEM, as shown in Fig. 3. Fig. 3a shows the sheet-like structure of the as-synthesized Bi_2MoO_6 sample. It can be seen that the sizes of Ag_3PO_4 crystals are of 10 - 20 nm (Fig. 3b). From Fig. 3c, it can be clearly found that the Ag NPs and Ag_3PO_4 NPs were loaded on the surface of Bi_2MoO_6. Fig. 3d shows the HRTEM image of the as-fabricated $Ag/Ag_3PO_4/Bi_2MoO_6$ sample. By measuring the lattice fringes, the resolved interplanar distances are about 0.236, 0.213, and 0.314 nm, which correspond to the (111) plane of Ag, the (210) plane of Ag_3PO_4, and the (131) plane of Bi_2MoO_6, respectively.

Fig. 4a displays the UV-vis diffuse reflectance spectra of Bi_2MoO_6, Ag_3PO_4, Ag/Bi_2MoO_6, Ag/Ag_3PO_4, Ag_3PO_4/Bi_2MoO_6, and $Ag/Ag_3PO_4/Bi_2MoO_6$. It can be seen that bare Bi_2MoO_6 exhibits strong absorbance in wavelengths shorter than 520 nm, and pure Ag_3PO_4 shows strong absorbance in wavelengths shorter than 510 nm. The Ag_3PO_4/Bi_2MoO_6 sample shows the similar absorption edge and a broader absorption in the visible region as comparison with pure Bi_2MoO_6. Ag/Bi_2MoO_6 and Ag/Ag_3PO_4 samples show obvious visible-light absorption, which can be attributed to the surface Plasmon resonance (SPR) of the loading Ag, further confirming the formation of Ag. The absorption curve of the $Ag/Ag_3PO_4/Bi_2MoO_6$ shows distinctly enhanced visible-light absorption compared to the pure Bi_2MoO_6 and Ag_3PO_4/Bi_2MoO_6 samples. According to the plot of $(ahv)^2$ versus energy, as shown in Fig. 4b, the band gap energies (E_g) of Ag_3PO_4 and Bi_2MoO_6 have been calculated to be 2.42 and 2.36 eV, respectively. The band structure of Ag_3PO_4 and Bi_2MoO_6 can be estimated according to the empirical equations 1 and 2 below;

$$E_{VB} = X - E^e + 0.5E_g \quad (1)$$

$$E_{CB} = E_{VB} - E_g \quad (2)$$

where E_{VB} is the valence band edge potential, E_{CB} is the conduction band edge potential, X is the electronegativity of the semiconductor, which is the geometric mean of the electronegativity of the constituent atoms, E^e is the energy of free electrons on the hydrogen scale (about 4.5 eV), E_g is the band gap energy of the semiconductor. Thus, the E_{VB} of Ag_3PO_4 and Bi_2MoO_6 are calculated to be 2.67 and 2.33 eV, respectively, and their corresponding E_{cB} are determined to be 0.25 and -0.31 eV, respectively. The results are in agreement with the reported works [28, 22]. The energy band structure diagram of Ag_3PO_4, Ag, and

View Article Online
DOI: 10.1039/C5RA22110B

Bi_2MoO_6 is thus schematically illustrated, as shown in Scheme 1. Under visible light irradiation, both Ag_3PO_4 and Bi_2MoO_6 are excited, and the photogenerated holes and electrons are in their conduction and valence band, respectively. The electrons on the CB of Ag_3PO_4 can easily shift into metal Ag (electron transfer I: Ag_3PO_4 CB → Ag) through the Schottky barrier because the CB potential of Ag_3PO_4 is more negative than the Fermi level of the loaded metal Ag. Meanwhile, the holes on the VB of Bi_2MoO_6 can also migrate to metal Ag (hole transfer II: Bi_2MoO_6 VB → Ag) because the Fermi level of Ag is more negative than the VB of Bi_2MoO_6, and then combine with the electron here. Therefore, simultaneous electron (I) and hole (II) transfers enhance the charge separation of Ag_3PO_4 and Bi_2MoO_6.

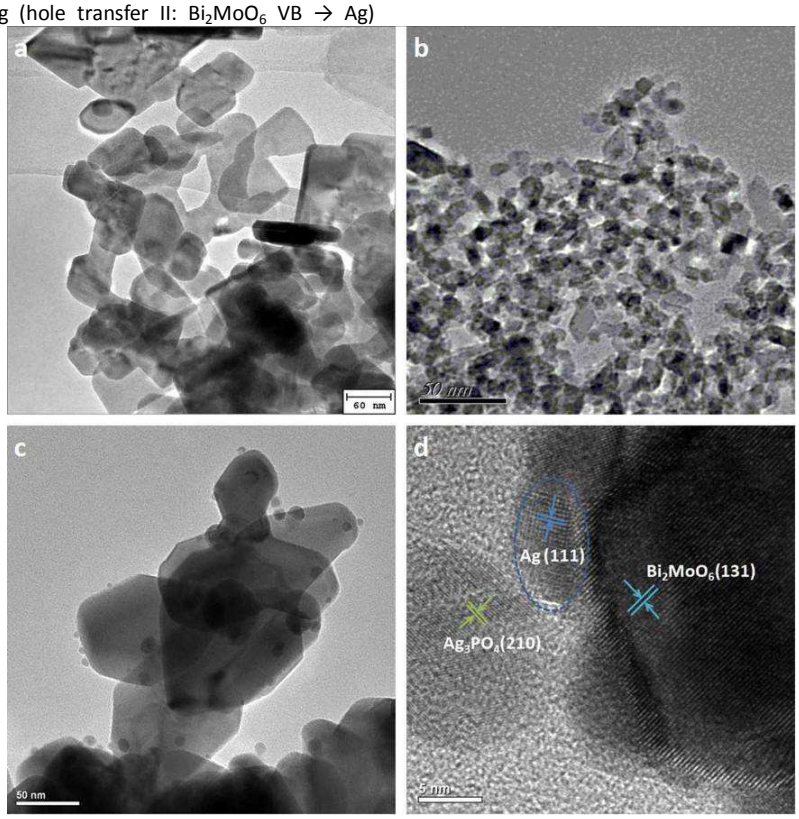

Fig. 3 TEM images of Bi_2MoO_6 (a), Ag_3PO_4 (b), $Ag/Ag_3PO_4/Bi_2MoO_6$ (c), and HRTEM image of $Ag/Ag_3PO_4/Bi_2MoO_6$ (d).

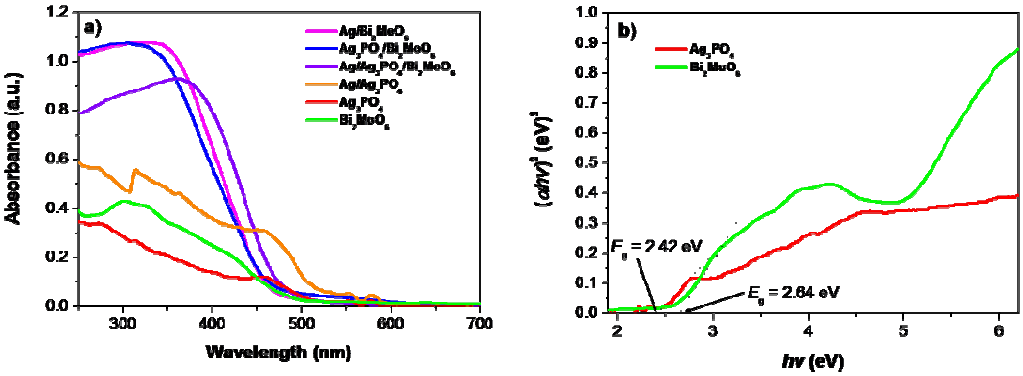

Fig. 4(a) UV-vis DRS of as-synthesized samples. (b) the plots of $(\alpha h\nu)^2$ versus photon energy ($h\nu$) for the band gap energies of Ag_3PO_4 and Bi_2MoO_6.

View Article Online
DOI: 10.1039/C5RA22110B

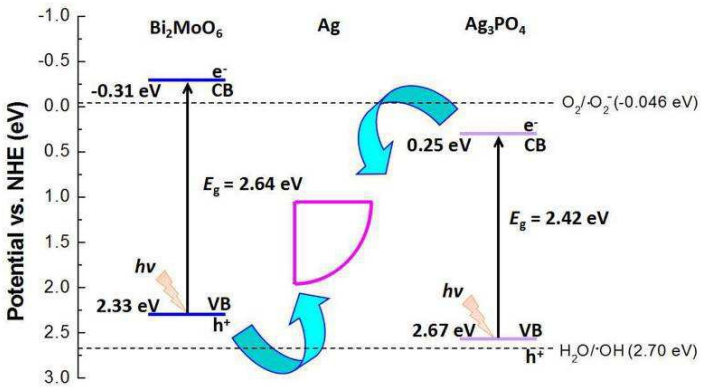

Scheme 1 Schematic diagram of the separation and transfer of photogenerated charges in the hybrid under visible light irradiation.

The photocatalytic properties of the as-prepared samples under visible light irradiation were evaluated, as shown in Fig. 5. This result clearly demonstrates that the $Ag/Ag_3PO_4/Bi_2MoO_6$ hybrid exhibited higher photocatalytic activity than pure Ag_3PO_4, Bi_2MoO_6, Ag/Ag_3PO_4, Ag/Bi_2MoO_6, and Ag_3PO_4/Bi_2MoO_6, which suggests that combining Ag/Ag_3PO_4 and Bi_2MoO_6 is an efficient route to enhance their photocatalytic activities. In the presence of $Ag/Ag_3PO_4/Bi_2MoO_6$, almost 100% of the Rh B molecules were decomposed within 80 min visible light irradiation. The Ag_3PO_4 NPs and Ag NPs coating can improve the visible light absorption efficiency (Fig. 4a), which is beneficial for the hybrid to photolyze Rh B. In addition, efficient Z-scheme system can separate the photoinduced charges effectively, thus enhancing the photocatalytic performance of $Ag/Ag_3PO_4/Bi_2MoO_6$.

The photoluminescence (PL) emission spectra were studied to investigate the charge recombination and transfer behaviour of the $Ag/Ag_3PO_4/Bi_2MoO_6$ photocatalyst, as shown in Fig. 6. It is well-known that the recombination of electron−hole pairs can release energy in the form of PL emission. In general, a lower PL intensity indicates lower recombination of charge carriers, leading to higher photocatalytic activity. However, the $Ag/Ag_3PO_4/Bi_2MoO_6$ with the higher photocatalytic activity showed a higher PL intensity than that of Bi_2MoO_6 and Ag_3PO_4/Bi_2MoO_6. The higher PL intensity of $Ag/Ag_3PO_4/Bi_2MoO_6$ would be resulted from higher recombination of photogenerated electron-hole pairs in the metallic Ag. The photogenerated electrons in the CB of Ag_3PO_4 and holes in the VB of Bi_2MoO_6 will shift to the metallic Ag simultaneously and then combine here, which leads to higher PL intensity. The recombination in the metallic Ag is benefical for accelerating the separation of the photogenerated electron-hole pairs in both Ag_3PO_4 and Bi_2MoO_6, so the photocatalytic performance of $Ag/Ag_3PO_4/Bi_2MoO_6$ improved. In addition, it can be clearly observed that the PL intensity of Ag_3PO_4/Bi_2MoO_6 was lower than that of pure Bi_2MoO_6 because of the formation of heterojunction between Ag_3PO_4 and Bi_2MoO_6 can efficiently suppress the recombination of the photogenerated electron−hole in the hybrid. On the basis of the above results, the $Ag/Ag_3PO_4/Bi_2MoO_6$ system is a typical Z-scheme photocatalyst rather than heterojunction photocatalyst. It is suggested that rich electrons in the CB of Bi_2MoO_6 and holes in the VB of Ag_3PO_4 participate in the reduction reaction of dissolved O_2 and the oxidation of Rh B, respectively. The stability and reusability of $Ag/Ag_3PO_4/Bi_2MoO_6$ photocatalyst were evaluated by the cycling degradation experiment, as shown in Fig. S2. The results revealed that the $Ag/Ag_3PO_4/Bi_2MoO_6$ did not show obvious decrease of photocatalytic degradation activity under visible light, indicating that the $Ag/Ag_3PO_4/Bi_2MoO_6$ hybrid photocatalyst is sufficient stable for photocatalytic degradation of Rh B.

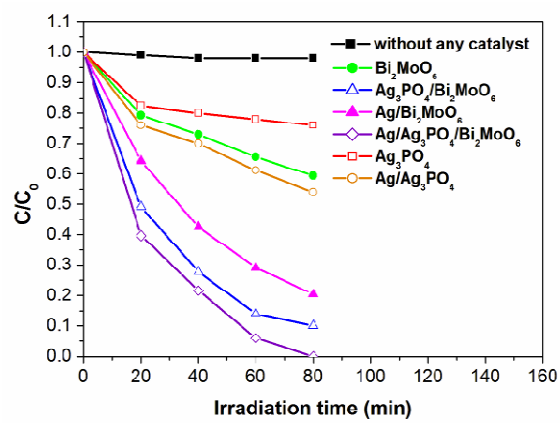

Fig. 5 Photodegradation efficiencies of Rh B as a function of irradiation time for different photocatalysts.

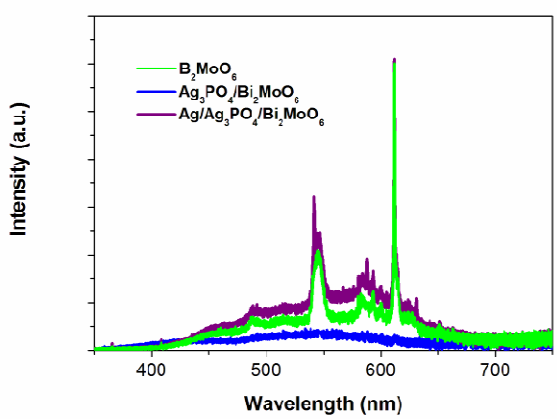

Fig. 6 Room temperature PL spectra of as-synthesized samples.

View Article Online
DOI: 10.1039/C5RA22110B

To investigate the photocatalytic mechanism of the $Ag/Ag_3PO_4/Bi_2MoO_6$ hybrid, the effect of scavengers on the degradation of Rh B was tested in the photocatalytic oxidation process and the results are shown in Fig. 7. As revealed in Fig. 7, under the visible-light irradiation of the $Ag/Ag_3PO_4/Bi_2MoO_6$ sample, the photodegradation rate of Rh B had slight decrease after the addition of hydroxyl radical scavenger IPA, indicating that •OH was not the main reactive specie in the photocatalytic process. In contrast, the photocatalytic degradation of Rh B was significantly repressed in presence of EDTA-2Na and BQ. According to these results, it can be concluded that h^+ and $O_2^{\bullet-}$ are the main oxygen active species for $Ag/Ag_3PO_4/Bi_2MoO_6$ photocatalyst in the Rh B solution under visible light illumination. It can be deduced that the electrons left on the E_{CB} of Bi_2MoO_6 reduce O_2 to $O_2^{\bullet-}$ through one-electron reducing reaction because the E_{CB} potential of Bi_2MoO_6 is more negative than $E_0(O_2/O_2^{\bullet-})$ (−0.046 eV vs. NHE). Both the holes in the E_{VB} of Ag_3PO_4 and the $O_2^{\bullet-}$ radicals can completely oxidize Rh B molecules to water and carbon dioxide.

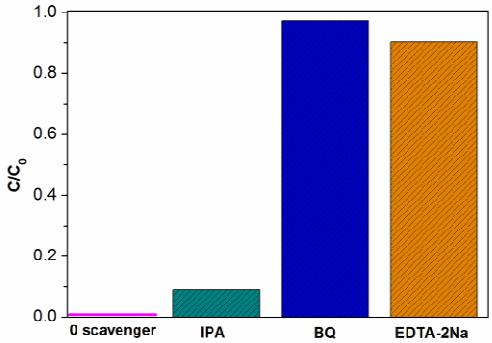

Fig. 7 Trapping experiments of active species during the photocatalytic degradation of Rh B over $Ag/Ag_3PO_4/Bi_2MoO_6$ sample under visible light irradiation.

4. Conclusions

A high-efficiency visible-light-driven $Ag/Ag_3PO_4/Bi_2MoO_6$ Z-Scheme photocatalyst was successfully synthesized through an in-situ precipitation process. The $Ag/Ag_3PO_4/Bi_2MoO_6$ hybrid photocatalyst displayed obviously superior photocatalytic performance than that of bare Ag_3PO_4, Bi_2MoO_6, Ag/Ag_3PO_4, Ag/Bi_2MoO_6, and Ag_3PO_4/Bi_2MoO_6 for the photo-degradation of Rh B under visible light irradiation. The superior photocatalytic activity of $Ag/Ag_3PO_4/Bi_2MoO_6$ may be resulted from the efficient separation of photogenerated electron-hole pairs through the Z-scheme system composed of Ag_3PO_4, Ag and Bi_2MoO_6. On the basis of the results of this study, the $Ag/Ag_3PO_4/Bi_2MoO_6$ hybrid photocatalyst is expected to be a useful visible-light photocatalyst for practical applications.

Acknowledgment

This work was supported by the Science and Technology Research Project of the Department of Education of Jilin Province (2015220).

References

1 M. R. Hoffmann, S. T. Martin, W. Choi and D. W. Bahnemannt, *Chem. Rev.*, 1995, **95**, 69.
2 Y. Mao and S. S. Wong, *J. Am. Chem. Soc.*, 2006, **128**, 8217.
3 R. Mohan, K. Krishnamoorthy and S. J. Kim, *Solid State Commun.*, 2012, **152**, 375.
4 L. Zhang, W. Z. Wang, S. M. Sun, Y. Y. Sun, E. P. Gao and Z. J. Zhang, *Appl. Catal. B Environ.*, 2014, **148–149**, 164.
5. W. Yao, B. Zhang, C. Huang, C. Ma, X. Song and Q. Xu, *J. Mater. Chem.*, 2012, **22**, 4050.
6. X. Ma, H. Li, Y. Wang, H. Li, B. Liu, S. Yin and T. Sato, *Appl. Catal. B Environ.*, 2014, **158**, 314.
7. W. Liu, M. Wang, C. Xu, S. Chen and X. Fu, *Mater. Res. Bull.*, 2013, **48**, 106.
8. L. Zhang, H. Zhang, H. Huang, Y. Liu and Z. Kang, *New J. Chem.*, 2012, **36**, 1541.
9. B. Cao, P. Dong, S. Cao and Y. Wang, *J. Am. Ceram. Soc.*, 2013, **96**, 544.
10 X. Li, R. Huang, Y. Hu, Y. Chen, W. Liu, R. Yuan and Z. Li, *Inorg. Chem.*, 2012, **51**, 6245.
11 H.F. Cheng, B.B. Huang, Y. Dai, X.Y. Qin and X.Y. Zhang, *Langmuir*, 2010, **26**, 6618.
12 X. Xiao and W.D. Zhang, *J. Mater. Chem.*, 2010, **20**, 5866.
13 G.P. Dai, J.G. Yu and G. Liu, *J. Phys. Chem. C*, 2011, **115**, 7339.
14 Y.F. Sun, B.Y. Qu, Q. Liu, S. Gao, Z.X. Yan, W.S. Yan, B.C. Pan, S.Q. Wei and Y. Xie, *Nanoscale*, 2012, **4**, 3761.
15 W.Z. Yin, W.Z. Wang and S.M. Sun, *Catal. Comm.*, 2010, **11**, 647.
16 M.Y. Zhang, C.L. Shao, J.B. Mu, X.M. Huang, Z.Y. Zhang, Z.C. Guo, P. Zhang and Y.C. Liu, *J. Mater. Chem.*, 2012, **22**, 577.
17 M.Y. Zhang, C.L. Shao, J.B. Mu, Z.Y. Zhang, Z.C. Guo, P. Zhang and Y.C. Liu, *CrystEngComm*, 2012, **14**, 605.
18 Y.L. Tian, B.B. Chang, J.L. Lu, J. Fu, F.N. Xi and X.P. Dong, *ACS Appl. Mater. Interfaces*, 2013, **5**, 7079.
19 M.Y. Zhang, C.L. Shao, P. Zhang, C.Y. Su, X. Zhang, P.P. Liang, Y.Y. Sun and Y.C. Liu, *J. Hazard. Mater.*, 2012, **225-226**, 155.
20 P.F. Wang, Y.H. Ao, C. Wang, J. Hou and J. Qian, *Carbon*, 2012, **5**, 5256.
21 J. Ren, W.Z. Wang, M. Shang, S.M. Sun and E.P. Gao, *ACS Appl. Mater. Interfaces*, 2011, **3**, 2529.
22 P. Zhang, C.L. Shao, M.Y. Zhang, Z.C. Guo, J.B. Mu, Z.Y. Zhang, X. Zhang and Y.C. Liu, *J. Hazard. Mater.*, 2012, **217–218**, 422.
23 G.H. Tian, Y.J. Chen, X.Y. Meng, J. Zhou, W. Zhou, K. Pan, C.G. Tian, Z.Y. Ren and H.G. Fu, *ChemPlusChem*, 2013, **78**, 117.
24 H.P. Li, J.Y. Liu, W.G. Hou, N. Du, R.J. Zhang and X.T. Tao, *Appl. Catal. B: Environ.*, 2014, **160-161**, 89.
25 Y. P. Bi, S. X. Ouyang, N. Umezawa, J. Y. Cao and J. H. Ye, *J. Am. Chem. Soc.,* 2011, **133**, 6490.

View Article Online
DOI: 10.1039/C5RA22110B

26 C. T. Dinh, T. D. Nguyen, F. Kleitz and T. O. Do, *Chem. Commun.*, 2011, **47**, 7797.
27 Y.S. Xu and W.D. Zhang, *Dalton Trans.*, 2013, **42**, 1094.
28 Z.H. Cheng, F. Bing, Q. Liu, Z.G. Zhang and X.M. Fang, *J. Mater. Chem. A.*, 2014, **00**, 1.
29 H. Katsumata, T. Sakai, T. Suzuki and S. Kaneco, *Ind. Eng. Chem. Res.*, 2014, **53**, 8018
30 Y.Y. Bu, Z.Y. Chen, and C.J. Sun, *Appl. Catal. B Environ.*, 2015, **179**, 363.

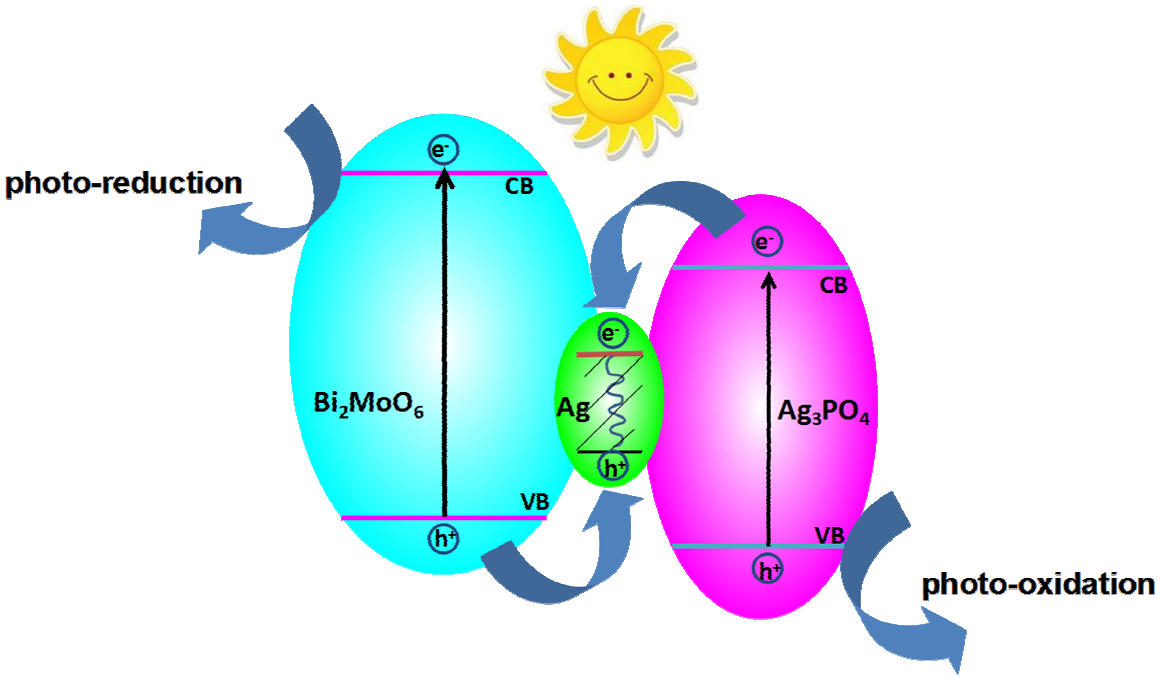

► A novel Z-Scheme $Ag/Ag_3PO_4/Bi_2MoO_6$ photocatalyst was successfully synthesized.

► $Ag/Ag_3PO_4/Bi_2MoO_6$ hybrid photocatalyst exhibited enhanced photocatalytic activity.